Pergamon

Journal of Structural Geology, Vol. 18, No. 1, pp. 121 to 130, 1996

0191-8141/96 $15.00 + 0.00

0191-8141(95)00081-X

Behaviour of spherical rigid objects and passive markers during bulk inhomogeneous shortening of a fluid

L. K. STEWART

Department of Earth Sciences, James Cook University, Townsville, Qld 4811, Australia

(*Received* 9 *August* 1994; *accepted in revised form* 13 *July* 1995)

Abstract—Quantitative analysis of the kinematics of an experimental, gravity-driven, inhomogeneous time-dependent flow showed that the kinematics of the flow varied both temporally and spatially. The variation in kinematics of the flow included vorticity rotation sense reversals and the results provide possible insight into the kinematics of gravity spreading flows. The variation of the kinematics reflected the influence of the boundary conditions upon the flow.

Spherical inclusions and thin, columnar, passive markers placed within the fluid prior to deformation also allowed the fluid flow to be used to examine some of the possible relationships that may form between porphyroblasts and passive foliations in inhomogeneous time-dependent flows. Comparison of initial and final orientations of several spherical inclusions suggested an apparent lack of rotation during deformation. Conversely, comparison of the initial and final orientation of passive strain markers placed in close proximity to these inclusions suggested a non-coaxial deformation environment rather than a coaxial environment. The apparent lack of rotation of these inclusions resulted from a reversal in their rotation sense during deformation of the system. The reversal in rotation sense of these inclusions was the result of time-varying levels of spin and shear induced vorticity.

During deformation, fold-like structures were produced in the passive markers. This allowed the flow to be used to examine possible relationships that may form between porphyroblasts and layers passively folded during inhomogeneous time-dependent flow. The inclusion/passive-marker relationships across the folds suggest that relationships between porphyroblasts (with inclusion trails) and foliations in rock layers, passively folded by an inhomogeneous time-dependent flow, may contain similar relationships to folds that formed by layer buckling. Knowledge of the level of passive behaviour of the layers and boundary conditions during this type of deformation is essential for utilizing porphyroblast/foliation geometry to evaluate deformation history.

INTRODUCTION

Several authors have conducted theoretical and experimental studies examining the behaviour of rigid objects and/or linear markers in fluids deformed by combinations of pure and simple shear and homogeneous deformation (Ghosh & Ramberg 1976, Ramberg & Ghosh 1977, Skjernaa 1980, Fernandez *et al.* 1983, Freeman 1985, Passchier 1987, Ildefonse *et al.* 1992). All geological deformation is inhomogeneous (Hobbs *et al.* 1976) and an experimental model was developed to examine the kinematics and spherical rigid object/passive marker behaviours within a particular type of inhomogeneous time-dependent flow.

In this study, two experiments were conducted by placing spherical inclusions and vertically oriented passive markers within a supported, clear, isotropic mass of viscous fluid. One other experiment was conducted with rigid marker particles placed within the fluid mass in addition to the inclusions and passive marker lines. Gravity was chosen as the driving force for the deformation, as gravitational spreading is thought to be an important geological process (Elliot 1976, Dewey 1988, Bell & Johnson 1989, Froitzheim 1992). To initiate an experimental deformation, the supports for the fluid mass were withdrawn and the system allowed to collapse under the effect of gravity.

This procedure resulted in an inhomogeneous time-dependent flow or, alternatively, deformation by bulk inhomogeneous shortening. Bell (1981) defined bulk inhomogeneous shortening (BIS) and divided it into two categories: (a) non-coaxial on the bulk scale where, during progressive shortening, there is rotation of a line, parallel to the average direction of shortening that connects the centres of the bulk boundaries under shear stress, and (b) coaxial on the bulk scale where, during progressive shortening, there is no rotation of a line parallel to the average direction of shortening that joins the centres of the bulk boundaries under shear stress. Coaxial bulk inhomogeneous shortening is equivalent to Ramsay's (1963) inhomogeneous form of pure shear (Bell 1981). At the scale of the experiments, the deformations can be described as having taken place by coaxial bulk inhomogeneous shortening. The flow and relationships modelled have possible application to: (1) gravity spreading flow; (2) porphyroblast and foliation relationships in inhomogeneous time-dependent flow; and (3) buckle folding.

The clear, viscous fluid and apparatus utilized in the experiments enabled the orientations with time of the inclusions and passive markers and the positions of marker particles to be photographically recorded for analysis (Fig. 1). The kinematics of the deformation in two dimensions were analysed using the computerized deformation analysis software Marker Analysis (Bons *et al.* 1993). The resulting progressive deformation field was used to quantify the kinematics of the gravity spreading flow and to provide a kinematic interpretation

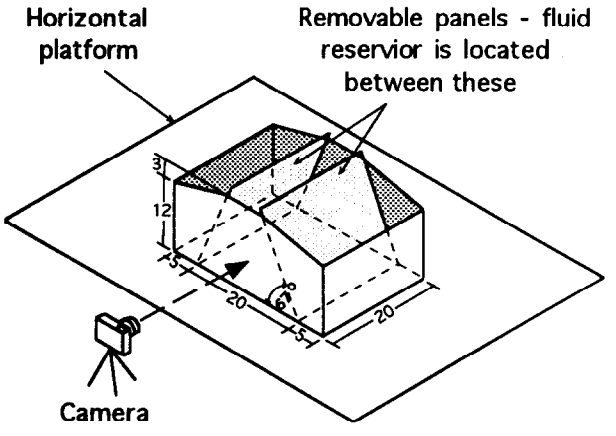

Fig. 1. Schematic diagram of the experimental apparatus showing dimensions, camera location and removable reservoir panels. The removable panels of the reservoir were inclined towards the centre at 67°.

of the observed motion of the inclusions and passive markers during deformation.

The inhomogeneous flow produced fold-like structures in the initially vertically oriented, passive markers. The relationships between the final orientations of the inclusions and passive markers across these folds, which have a known deformation history, have possible application to the relationships between porphyroblasts and foliations in folded rocks. Important implications with regard to determination of deformation history from porphyroblast and foliation relationships are discussed.

EXPERIMENTAL APPARATUS

The experimental apparatus consisted of a clear polycarbonate container with a horizontal base of dimensions 20 × 30 cm and height 15 cm (Fig. 1). The sides of the container and the two removable panels formed a reservoir for the fluid to be used in the experiment. The two removable panels were inclined toward the centre of the apparatus at 67°. The degree of inclination of these panels was chosen to: (a) allow sufficient distance for the extension of the fluid mass during collapse before contact with the container limits and (b) restrict the total volume of the fluid mass, necessitated by problems relating to the acquisition of raw materials used in its manufacture. The fluid used was a clear, viscous, borate cross-linked polyvinyl alcohol gel (Casassa *et al.* 1986) with a viscosity of the order of 2.5×10^3 Pa s^{-1} at a strain rate of 3×10^{-2} s^{-1}. The fluid showed a linear relationship between shear stress and strain rate over the range of strain rates generated (up to 3.43×10^{-2} s^{-1}) during the experimental deformations. At strain rates above 5×10^{-2} s^{-1}, the relationship between shear stress and strain rate in the fluid becomes non-linear. The fluid is water based and dehydration in use and storage resulted in variations in the fluid's viscosity and differing experimental durations. However, the variation in experimental duration did not effect any change in the observed behaviour of inclusions or markers (e.g. rotation sense reversals).

Inclusions and passive strain markers

The experiments utilized rigid spherical inclusions of acrylic construction, with a diameter of approximately 5 mm. The hemispheres of each inclusion were painted a different colour, which allowed the orientation of each sphere to be determined during deformation. A cylindrical hole of diameter 0.5 mm through the centre of each inclusion was necessary to allow emplacement of the inclusions within the gel. These holes were oriented vertically at the commencement of the experiments. The inclusions were neutrally buoyant in the gel within the time span of the experiments, with a rise rate of 14.4 mm per day. Two vertical columns of inclusions were placed within the fluid mass with five inclusions uniformly distributed within each column. The inclusions were located in a vertical, planar cross-section of the fluid parallel to the container front. Passive strain markers were used to examine the progressive strain and amount of apparent rotation within the fluid near the inclusions. These markers consisted of thin dye lines placed within the system by coating a straight length of 0.5 mm diameter wire with ink, pushing it into the gel and then removing it. The passive marker lines were oriented vertically and placed within 5 mm of the columns of inclusions (Fig. 2).

Data acquisition and analysis

An undistorted view of the deformation of the planar cross-section containing the inclusions and markers was possible from the camera location shown in Fig. 1. Removal of the two inclined panels allowed gravity-driven deformation of the fluid mass to commence. A 35 mm power advance camera, with its focal plane oriented parallel to the side wall of the container, recorded the motion of the inclusions and passive markers at 2 s intervals during the deformation process. To avoid further complication of the boundary conditions (see below), the first contact of the gel's flow front with the ends of the container signalled the end of data collection (Fig. 3).

The resulting photographs provided the orientation, with time, of the inclusions and markers during deformation. The angle of the tangent to the strain marker portion in closest proximity to an inclusion gave the strain marker orientation at that location. This allowed comparison of the apparent rotation sense of the fluid (as suggested by passive marker rotation) with the physical rotation of the inclusion. Incorporation of marker particles into the fluid cross-section containing the inclusions allowed quantitative analysis of the deformation kinematics using the program Marker Analysis (Bons *et al.* 1993). This software package allows the analysis and visualization of deformation in see-through experiments that contain marker particles.

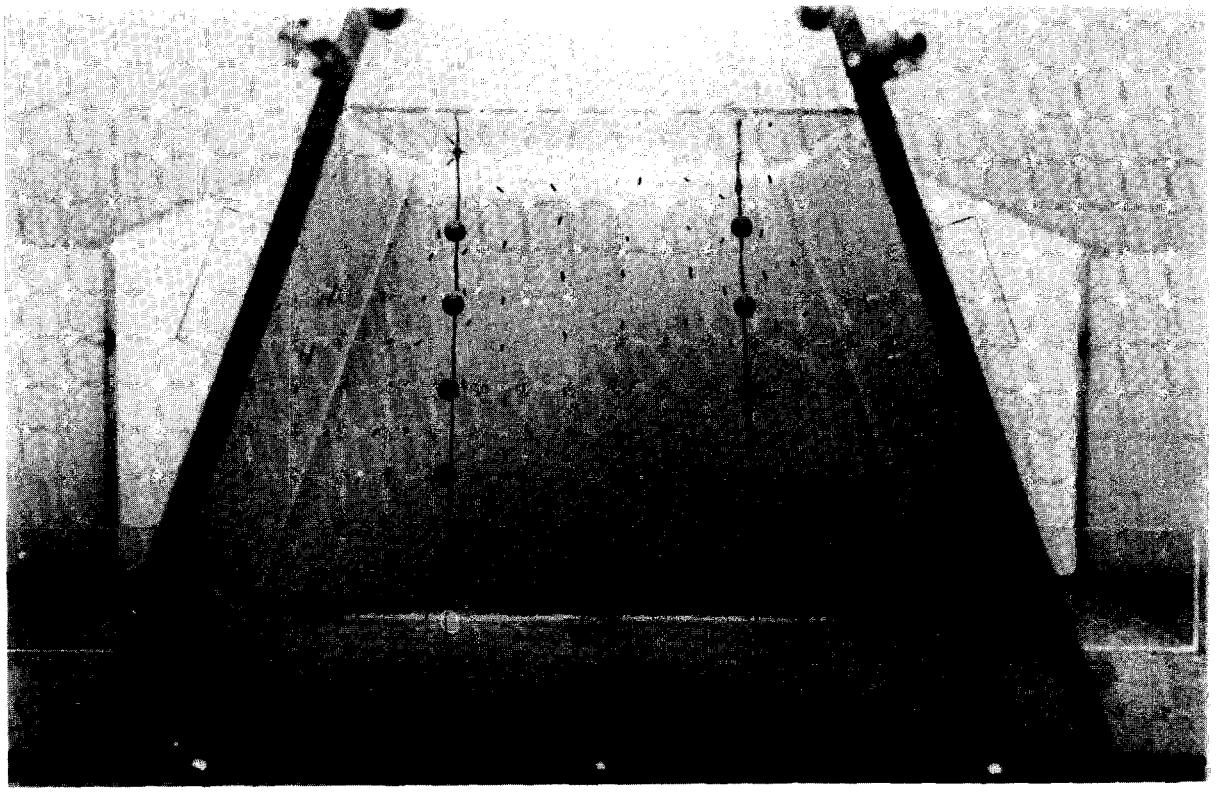

Fig. 2. Photograph of apparatus before commencement of an experiment. The vertical columns of spherical inclusions and nearby strain markers are visible within the viscous fluid mass located between the inclined panels. The spherical inclusions and marker particles are located in a planar cross-section parallel to the front of the container.

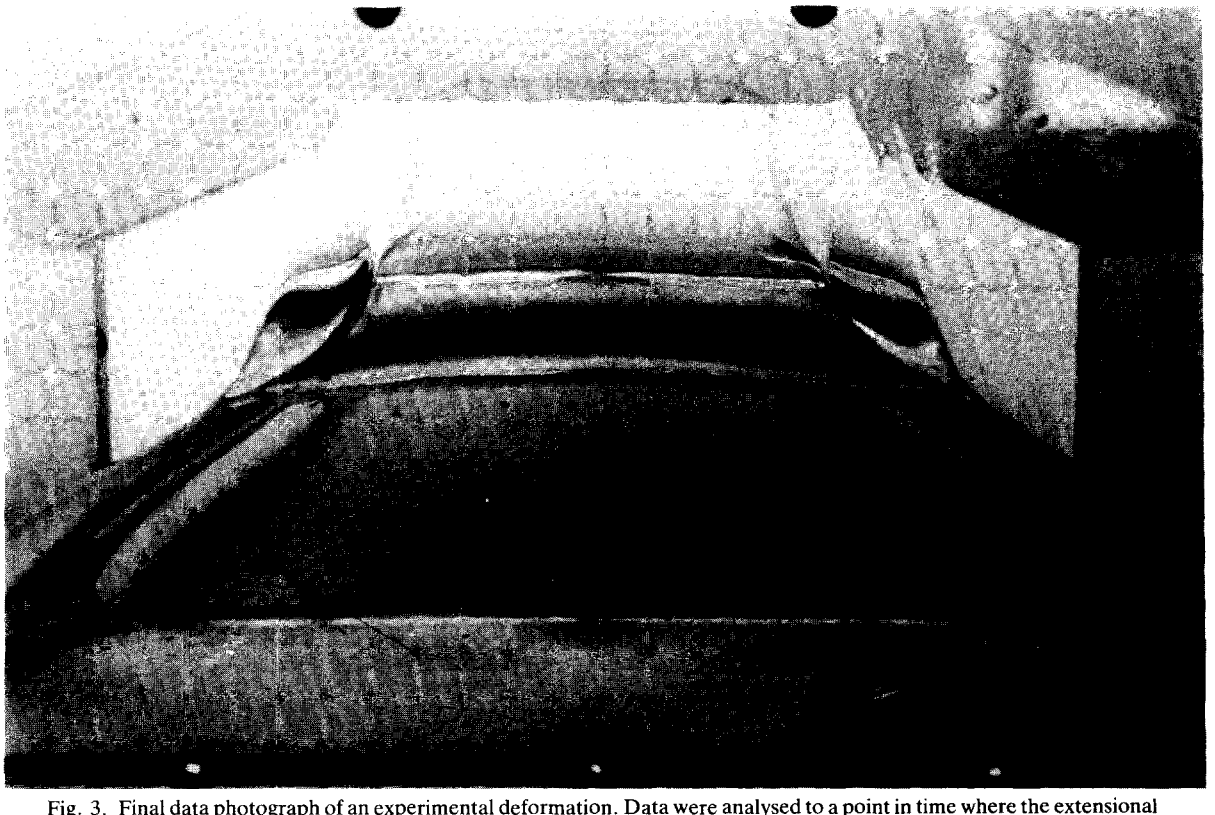

Fig. 3. Final data photograph of an experimental deformation. Data were analysed to a point in time where the extensional flow front of the fluid contacted the ends of the container. The duration of this experiment was 38 s. Note the fold-like structures that developed in the passive marker during deformation.

Boundary conditions

The boundary conditions for this viscous-spreading (Elliot 1976, Ramberg 1977) model consisted of a free upper surface combined with base and lateral boundaries that allowed no slip. Such boundary conditions were employed by Brun and Merle (1986) in their experimental examination of strain patterns in spreading–gliding nappes.

RESULTS

Analysis of inclusion and marker orientation data for the three experiments suggested a distinct variation in the kinematics between the upper and lower portions (Fig. 4) of the flowing fluid mass. Over the three experiments, 13 of the 14 inclusions (93%), located in the upper portions of the fluid mass, displayed a rotation sense reversal. However, the strain markers in both the upper and lower portions did not display a reversal in rotation sense during deformation. A comparison of passive marker and inclusion rotational behaviour, for markers and inclusions within the area of fluid in the upper left-hand portion of the system is shown in Fig. 5. Inclusions in the lower portions of the fluid mass rotated in the same sense as the passive markers (Fig. 6). The magnitude of the rotation of each inclusion was less than that of the marker.

Between experiments, there was some variation in the amount of rotation of both marker and inclusion at each individual location. In the case of the marker, this variation can be attributed to the placement error (±3°) for the initial vertical orientation of the marker. The variation in the level of rotation of inclusions at a location can be attributed to the error associated with placing the inclusion in the desired location (±4 mm).

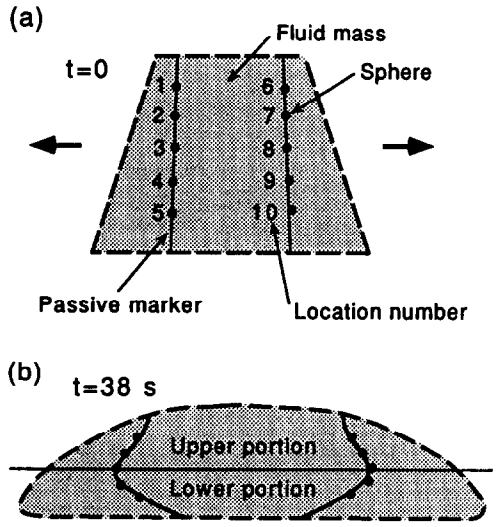

Fig. 4. Diagrammatic representation of (a) numbered inclusion locations and (b) delineation of deformed fluid mass into upper and lower portions. The area referred to as the upper portion lies above the line through the apex of the curved structure induced into the passive marker by the deformation and the lower portion lies below that line.

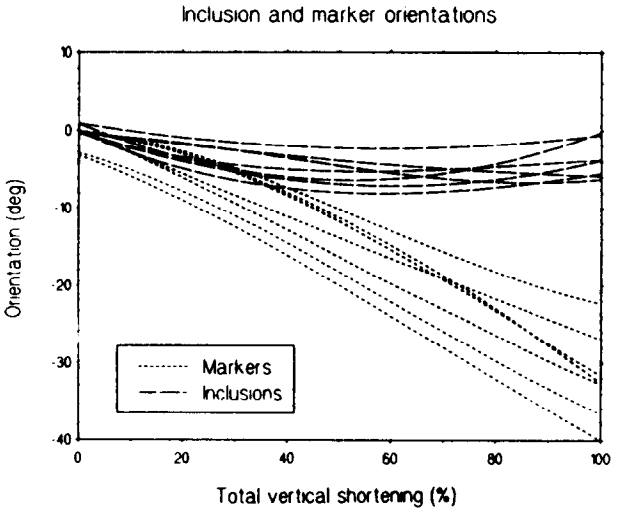

Fig. 5. Graph displays best-fit curves for inclusion and strain marker orientation, with time, for the inclusions and markers in the left-hand side of the upper portion over the three experiments. The inclusions displayed a reversal in rotation sense while the strain markers rotated in one sense for the duration of the experiment.

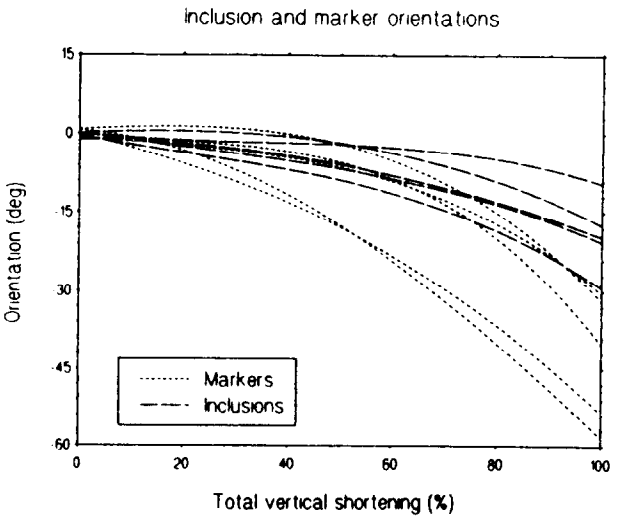

Fig. 6. Graph displaying best-fit curves for strain marker and inclusion orientation, with time, for inclusions and markers in the right-hand side of the lower portion over the three experiments. Inclusions in this location displayed rotation in the same sense as the strain marker. Rotation of inclusions in one sense, consistent with strain marker behaviour, was the norm for inclusions in the lower portions of the fluid mass.

At some locations, the inclusions and passive markers showed little rotational behaviour during deformation This suggests that deformation was virtually coaxial at these locations. These locations coincided with the apex of the curved structure induced into the strain marker by the deformation (Figs. 3 and 4).

DEFORMATION KINEMATICS

Upper portion of fluid mass

The reversal in rotation sense of the inclusions contained within the upper portion of the fluid mass is

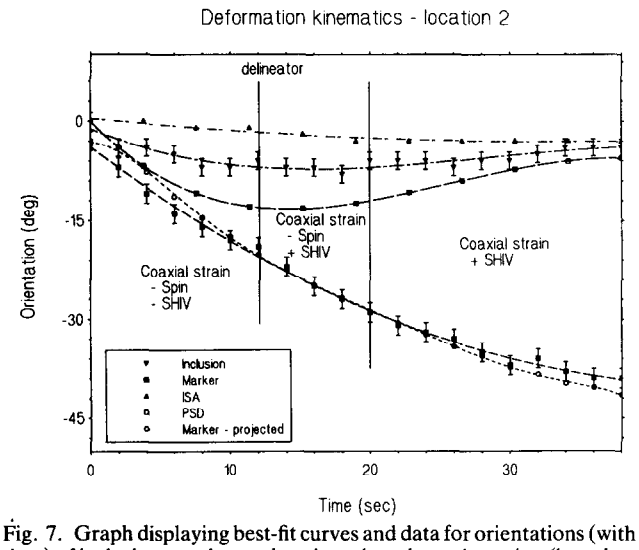

Fig. 7. Graph displaying best-fit curves and data for orientations (with time) of inclusion, marker and projected marker orientation (based on coaxial components of deformation) at location 2. Also shown are the orientations with time of the ISA and PSD, relative to their initial orientations, at location 2.

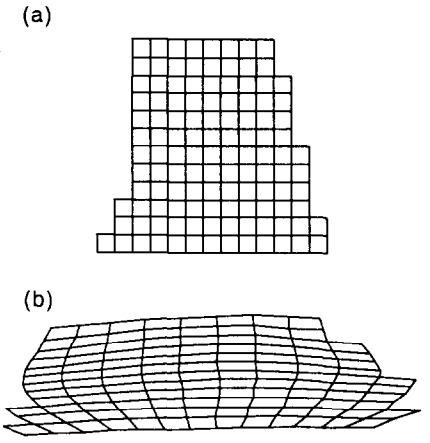

Fig. 8. Undeformed (a) and deformed (b) grids for the experiment incorporating marker particles. Considerable flattening is evident in the deformation of the fluid mass. The grids were produced using the Marker Analysis software (Bons *et al.* 1993).

related to the temporal and spatial variation in the levels of spin and shear induced vorticity (Lister & Williams 1983). Figure 7 shows a plot of inclusion and marker orientation with time for a location in the upper portion of the fluid mass (location 2, Fig. 4). This location was chosen for analysis because behaviour of the inclusion and marker were considered representative for that observed in the upper portion.

The experiment from which the data in Fig. 7 were obtained also had small marker particles distributed within the fluid cross-section containing the inclusions and passive markers (Fig. 2). The marker particles allowed quantitative analysis of the deformation using the marker analysis software. Data pertaining to the orientation with time of both the instantaneous stretching axis and the principal stretching directions of the strain ellipse, in the external reference frame, for the local area of fluid containing the inclusion, are also displayed in Fig. 7.

Ramsay (1962) noted that a foliation can rotate with respect to a stationary object in a progressive pure shear deformation. The experimental deformations involved a large component of vertical shortening (Fig. 8). Therefore, in any time interval, the shortening would produce a certain amount of rotation of the passive marker, provided that the initial marker orientation was not parallel to an extensional apophysis (Passchier 1987). The vertical shortening would not rotate the inclusion because spherical objects are irrotational in coaxial flow (Ghosh & Ramberg 1976, Passchier 1987).

The presence of marker particles in the system allowed the amount of vertical shortening across the location of an inclusion to be determined for each time interval. These shortening data, combined with the marker orientation at the beginning of each time interval, allowed calculation of the expected rotation of the marker due to vertical shortening only, in each time interval. Assuming constant area in cross-section during deformation, the following equation can be derived for the expected orientation of the marker line, due to vertical shortening only, at the end of a time interval:

$$\theta_2 = \tan^{-1}\left(\left(\frac{l_1}{l_2}\right)^2 \tan\theta_1\right) \quad (1)$$

where θ_2 is the passive marker orientation at the end of the time interval; θ_1 is the passive marker orientation at the beginning of the time interval; l_1 is the vertical separation of marker particles at the beginning of the time interval; and l_2 is the vertical separation of the marker particles at the end of the time interval.

Equation (1) is equivalent to Harker's (1886) equation and can also be derived through modification of Flinn's (1962) equation 23(a) for deformation of random orientations of lines during finite homogeneous strain. Use of the best-fit curve data for the shortening and marker-orientation values at each time point allowed a smoother and more accurate calculation of the expected orientation of the marker for each time interval. Figure 7 shows the expected orientations of the marker at the end of each time interval, due to the coaxial component of the deformation during that interval, as the 'Marker-projected' trace (note: each point represents the expected orientation of the marker after one time interval, based on the marker orientation at the beginning of that interval).

Examination of Fig. 7 shows that, up to $t = 12$ s, the change in orientation of the inclusion was in the same sense as the change in orientation of the principal stretching directions (PSD) and instantaneous stretching axes (ISA) of the local area of fluid surrounding the inclusion cross-section. The rotation with time of the PSD and inclusion indicates the presence of vorticity. The ISA spin during the first half of the deformation was in the same sense as the inclusion and PSD rotation. Shear induced vorticity (SHIV) is evident, in addition to spin, as both the PSD and inclusion rotate relative to the ISA. The PSD and inclusion rotated relative to the ISA until approximately $t = 12$ s, suggesting that the SHIV

was of decreasing magnitude. Comparison of the trace of actual marker orientation with the trace of projected marker orientation up to $t = 12$ s provides a visual indicator of the effect of the SHIV component upon marker orientation during this period. The SHIV caused a larger angular change in marker orientation to be recorded, over each time interval, than would be caused by the effect of shortening alone. The experimental flow up to $t = 12$ s can be classed as spinning, non-coaxial and rotational (Lister & Williams 1983).

In the period from approximately $t = 12$ s to $t = 20$ s (Fig. 7), the ISA continued to spin in an anti-clockwise sense. The PSD rotation sense indicates that the SHIV component was of clockwise sense in the period. The inclusion, in this period, rotated very little in the external reference frame. Also, the trace of projected orientation of the marker matched the trace of actual marker orientation. These factors indicate that the rotation of inclusion and marker, due to spin in an anti-clockwise sense, was countered almost exactly by SHIV of clockwise rotation sense during this period.

From approximately $t = 20$ s to the end of the deformation there is little further ISA spin. Continuing SHIV, of clockwise rotation sense, is evident as the inclusion and PSD rotated clockwise relative to the ISA (and thus the external reference frame). The effect that this SHIV component had upon marker orientation can be seen by comparing the traces of observed and projected marker orientations in the period. The changes in orientation, within each time interval, of the marker are smaller in magnitude than the projected change's orientation. The clockwise rotation sense of the SHIV caused a smaller angular change in marker orientation to be recorded, over each time interval, than would be caused by the effect of shortening alone. This resulted in a decrease in the observed rotation rate of the marker, but did not reverse the marker's rotation sense. Thus, the observed rotation sense of the inclusion was of opposite sense to that of the marker. The flow from $t = 20$ s to $t = 38$ s can be classed as non-spinning, non-coaxial and rotational (Lister & Williams 1983).

Velocity vector plots were produced for the deforming fluid mass at times $t = 2$ s and $t = 38$ s (Figs. 9a & b). The zero velocity reference point chosen for the plots coincided with the actual area of the fluid mass that had little velocity as measured in the external reference frame.

At $t = 2$ s (Fig. 9a) the plots reveal a vertical gradient, in the horizontal component of the fluid velocities. This horizontal component increases in magnitude from the upper and lower boundaries towards the middle of the fluid mass. No significant horizontal gradient in the vertical components of the fluid velocity can be seen. In the upper left-hand portion (incorporating location 2), the fluid velocity gradient would produce a SHIV component with an anti-clockwise rotation sense. At $t = 38$ s (Fig. 9b), the velocity plots in the upper left-hand portion now show a pronounced vertical gradient in horizontal velocity components, increasing from the lower boundary to the upper boundary. There is also a horizontal gradient in the vertical velocity components. In the upper left-hand portion, both of these spatial velocity gradients produced SHIV of clockwise rotation sense. This SHIV produced rotation of the inclusion in the opposite sense to that initially observed.

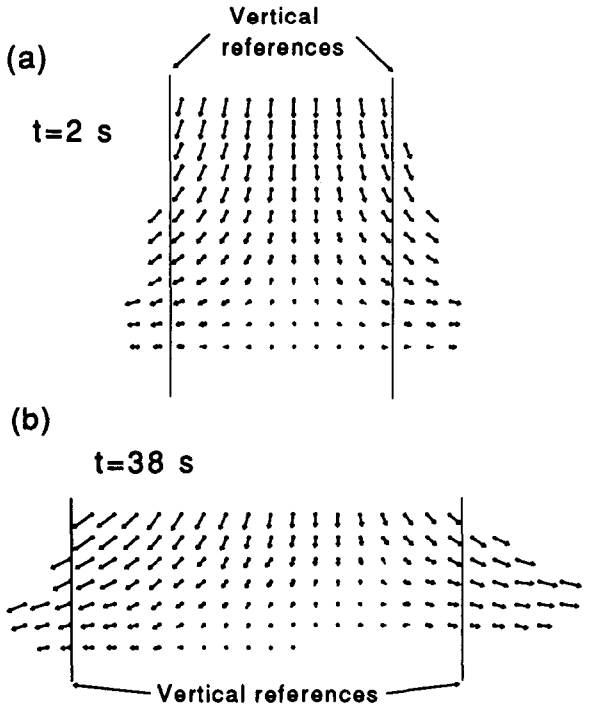

Fig. 9. Velocity vector plots for the gravity spreading flow at (a) $t = 2$ s and (b) $t = 38$ s. Vertical reference lines have been added to make the velocity gradients easier to view. The velocity plots were produced using the Marker Analysis software (Bons *et al.* 1993).

Lower portion of fluid mass

Inclusions contained within the lower portion of the deforming fluid mass displayed a single rotation sense. The behaviour of these inclusions can be explained by variation of the deformation kinematics with time. Figure 10 shows the observed orientations of a passive marker and inclusion (at location 10, Fig. 4) in the lower portion of the fluid mass. Also shown in Fig. 10 are ISA and PSD rotations and the projected orientation of the passive marker. This location was chosen for analysis as it was close to the base of the apparatus (where the non-coaxiality of the flow was greatest) and behaviours at this location were representative of those observed in the lower portion.

Examination of Fig. 10 shows that, as in the upper portion of the deforming fluid mass, there was a period of ISA spin, in the same sense as the inclusion and PSD rotation. The presence of a SHIV component is obvious as the PSD and inclusion rotated relative to the ISA. The effect of the SHIV component upon marker orientation can be seen by comparing the trace of observed marker orientation with the trace of projected orientation. The SHIV caused a greater angular change in marker orientation to be recorded, over each time interval, than

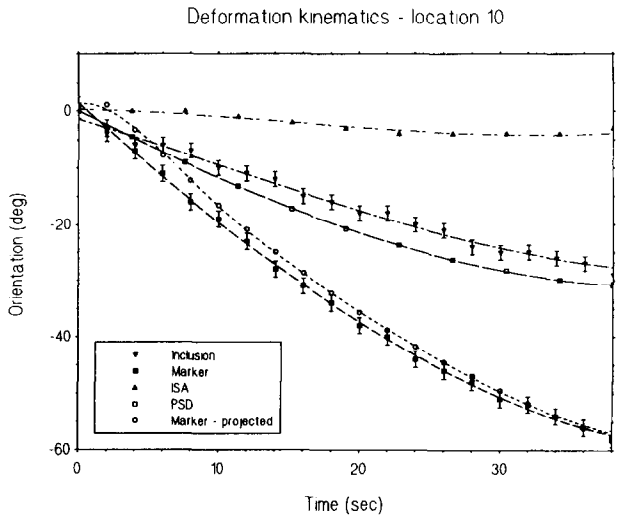

Fig. 10. Graph displaying best-fit curves and data for orientations (with time) of inclusion, marker and projected marker orientation (based on coaxial component of the deformation only) at location 10. Also shown are the orientations with time of the ISA and PSD, relative to their initial orientations, at location 10.

would be caused by the effect of shortening alone. At around t = 30 s, the ISA spin became negligible. From approximately $t \approx 32$ s, the rotation rate of inclusion and PSD slowed, and the projected marker trace nearly matched the actual marker trace. This means that the SHIV component decreased and the deformation was becoming more coaxial. However, as the conclusion of the experiment occurred at t = 38 s, there are not sufficient data points remaining in the set to make statements pertaining to the trend on kinematics during this period. The deformation between $t = 0$ and $t = 32$ s can be classed as spinning and non-coaxial and between t = 32 s and t = 38 s as non-spinning and non-coaxial (Lister & Williams 1983).

The velocity vector plots (Figs 9a & b) revealed a consistent vertical gradient in the horizontal components of fluid velocity in the lower right-hand portion (which incorporated location 10) at both $t = 2$ s and $t =$ 38 s. At $t = 38$ s (Fig. 9b), a slight horizontal gradient is evident in the vertical velocity components. These velocity gradients produced the SHIV component that rotated the inclusion during the deformation.

The difference in kinematics between the upper and lower portions reflected the imposed boundary conditions. The constrained lower boundary meant that elements of fluid at the lower boundary must have zero velocity. This resulted in a consistent gradient in fluid velocities between this boundary and the line of greatest fluid extension (a line joining the curved structures introduced into the passive markers by deformation). Fluid elements on the upper boundary were not constrained and thus fluid velocity gradients between the upper boundary and the line of greatest fluid extension could vary as deformation progressed.

DISCUSSION

Inclusion/marker relationships

The experiments allowed examination of the possible kinematics of a gravity spreading flow. The results reveal that the kinematics of a gravity spreading flow can be complex involving temporal and spatial variation of the levels of spin and shear induced vorticity. The results also suggest that boundary conditions are an important factor influencing the spatial variation of the kinematics in such flows.

Considering the inclusions and passive markers contained within the deforming fluid as analogous to spherical porphyroblasts and passive foliations allowed the examination of some of the possible relationships that may form between such entities within an inhomogeneous, time-dependent flow. In many cases, foliations within deformed rocks have been considered to behave as passive markers (Ghosh & Ramberg 1976, Boulter 1980, Gray 1981). However, not all foliations can be considered to act passively (Williams and Schoneveld 1981, Bell 1981, 1985). Because of this, the nature of the experiments outlined herein only allow us to examine the relationships between rigid objects and passive markers.

The relationship between foliations and other potential passive markers such as appendages of recrystallized material, and rigid objects such as porphyroblasts (with inclusion trails) and porphyroclasts, have been used to infer rigid object rotation sense (Spry 1963, Rosenfeld 1970, Schoneveld 1977, Powell & Vernon 1978, Passchier 1987, 1988) and as vorticity indicators (Cobbold & Gapais 1987, Passchier 1987). The experimental results suggest that during some inhomogeneous time-dependent flows it is possible for porphyroblasts (with inclusion trails) and a foliation to rotate in opposite senses during deformation while at other locations within the flow porphyroblasts could rotate in the same sense as the foliation. The rotation of porphyroblast and foliation in opposite senses would result from the rotation of the foliation, relative to the porphyroblast, due to the coaxial component of deformation (Ramsay 1962). The maximum amount of this rotation depends on the initial orientation of the foliation to the compressional ISA but is limited to 90° for a single shortening event. Porphyroblasts that rotated in the opposite sense to the foliation would record greater curvature in inclusion trial geometry than those that rotated in the same sense as, but not more than, the foliation. Examination of the inclusion trails within such porphyroblasts could lead to the incorrect assumption that there were higher levels of SHIV associated with the formation of the porphyroblasts that recorded the greater curvature in inclusion trail geometry.

Another possible application of the modelled inhomogeneous flow relates to the interpretation of inclusion marker relationships around passive folds. The post-deformation geometry of the passive markers (Fig. 3) suggests that if the passive markers were replaced with

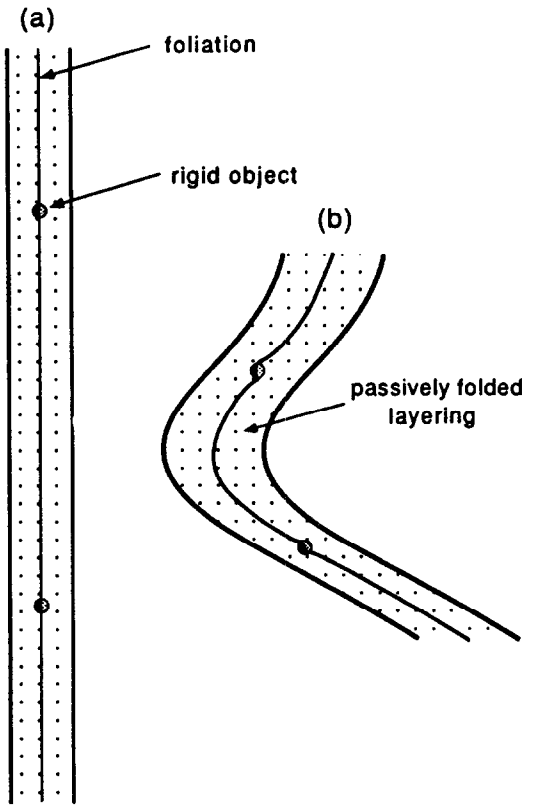

Fig. 11. Passive fold structure and inclusion/foliation relationships (extrapolated from experimental observations) (a) before deformation and (b) that may develop during inhomogeneous time-dependent flow. The inclusion/marker relationship in the upper limb of (b) suggests greater rotation of this inclusion than the one in the lower limb. In fact, relative to geographic coordinates, the opposite is true.

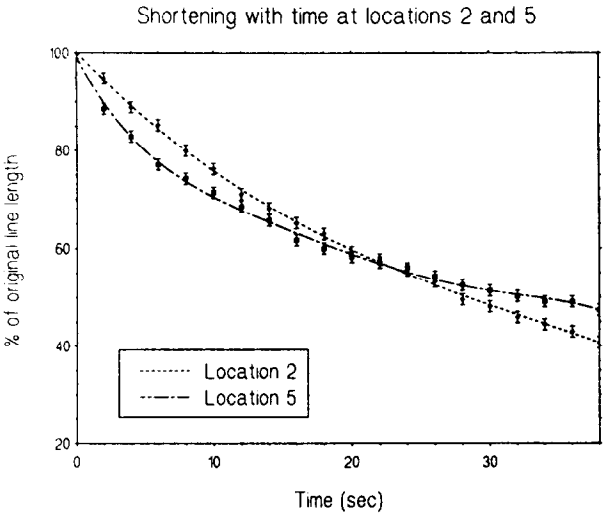

Fig. 12. Plots of vertical shortening with time at inclusion locations 2 and 5.

near-vertically oriented passive layers (plane of layers perpendicular to camera focal plane), then those passive layers would be folded during the flow. Assuming that the relative fluid velocity at the surface of an inclusion with respect to the inclusion will be zero, unless there is slip, the inclusion/marker relationship shown in Fig. 11 can be extrapolated. Without the knowledge that the fold in the layer formed passively in an inhomogeneous flow, different interpretations could be placed on the deformation history.

If the layer was assumed non-passive, the inclusion/marker relationship (Fig. 11b) could suggest compression of the layer that gave rise to rotation of the lower and upper limbs as in buckling (Biot 1961, Ramberg 1963) combined with flexural flow within the limbs (Hobbs *et al.* 1976). In this interpretation, flexural flow within the layer produces shear that causes inclusion rotation in the opposite sense to the rotation of the limb due to buckling (Visser & Mancktelow 1992). Also, analysis of the amount of shortening at inclusion locations in both the lower and upper portions of the fluid mass (Fig. 12) showed that there were only small differences in the amount of shortening with time at these locations. This means that the limbs of the fold extrapolated in Fig. 11(b) would have undergone similar amounts of shortening. The thinner, lower limb (measured normal to layering) is the result of higher levels of SHIV in that area. However, if the layer in Fig. 11(b) were considered non-passive, this may not be apparent and the difference in layer thickness could be attributed to competency variations along the layer's length. If the layer was assumed to have behaved passively, the inclusion/marker relationships would suggest a deformation environment in which there was ongoing spatial and temporal variation in the kinematics of deformation.

The experiments indicate that a simple-shaped passive fold, generated in an inhomogeneous time-dependent flow, can result from complex spatial and temporal variation in the deformation kinematics. As such, without definitive data indicating homogeneous or inhomogeneous deformation and whether there was buckling or passive behaviour of the layers during deformation, it may be difficult to relate inclusion/marker relationships (such as porphyroblast/foliation relationships) to deformation history in deformed rocks.

Acknowledgements—I wish to acknowledge the invaluable guidance of Dr Tim Bell. Reviewers Drs Benoit Ildefonse and Neil Mancktelow are thanked for their constructive comments that have resulted in a much improved manuscript. Thanks to Dr Brett Davis for pre-submission reviews of the manuscript and his helpful suggestions. Drs Paul Bons and Mark Jessell are thanked for their assistance with the superb deformation-analysis program they have developed, which they distribute freely to interested persons. I thank Phil McGuire, Paul Givney and Jim Darley for their assistance in the construction and preparation of the experimental rig. Also, I wish to thank all those who offered constructive suggestions during this study.

REFERENCES

Bell, T. H. 1981. Foliation development—the contribution, geometry and significance of progressive, bulk, inhomogeneous shortening. *Tectonophysics* **75**, 273–296.

Bell, T. H. 1985. Deformation partitioning and porphyroblast rotation in metamorphic rocks: a radical reinterpretation. *J. Metamorph. Geol.* **3**, 109–118.

Bell, T. H. & Johnson, S. E. 1989. Porphyroblast inclusion trails: the key to orogenesis. *J. Metamorph. Geol.* **7**, 279–310.

Biot, M. A. 1961. Theory of folding of stratified viscoelastic media and

its implications in tectonics and orogenesis. *Geol. Soc. Am. Bull.* **72**, 1595–1620.

Bons, P. D., Jessell, M. W. & Passchier, C. W. 1993. The analysis of progressive deformation in rock inclusions. *J. Struct. Geol.* **15**, 403–411.

Boulter, C. A. 1980. On the production of two inclined cleavages during a single folding event; Stirling Range SW Australia. *J. Struct. Geol.* **1**, 207–209.

Brun, J. P. & Merle, O. 1986. Strain patterns in models of spreading–gliding nappes. *Tectonics* **4**(7), 705–719.

Casassa, E. Z., Sarquis, A. M. & Van Dyke, C. H. 1986. The gelation of polyvinyl alcohol with borax. *J. Chem. Ed.* **63**, 57–60.

Cobbold, P. R. & Gapais, D. 1987. Shear criteria in rocks: an introductory review. *J. Struct. Geol.* **9**, 521–523.

Dewey, J. F. 1988. Extensional collapse of orogens. *Tectonics* **7**(6), 1123–1139.

Elliot, D. 1976. The energy balance and deformation mechanisms of thrust sheets. *Phil. Trans. R. Soc. Lond.* **A283**, 289–312.

Fernandez, A., Feybesse, J. L. & Mezure, J. F. 1983. Theoretical and experimental study of fabric developed by different shaped markers in two-dimensional simple shear. *Bull. Soc. géol. Fr.* **25**, 319–326.

Flinn, D. 1962. On folding during three-dimensional progressive deformation. *Q. J. geol. Soc. Lond.* **118**, 385–433.

Freeman, B. 1985. The motion of rigid ellipsoidal particles in slow flows. *Tectonophysics* **113**, 163–183.

Froitzheim, N. 1992. Formation of recumbent folds during synorogenic crustal extension (Austroalpine nappes, Switzerland). *Geology* **20**, 923–926.

Ghosh, S. K. & Ramberg, H. 1976. Reorientation of inclusions by combinations of pure and simple shear. *Tectonophysics* **34**, 1–70.

Gray, D. R. 1981. Compound tectonic fabrics in singly folded rocks from southwest Virginia, U.S.A. *Tectonophysics* **78**, 229–248..

Harker, A. 1886. On slaty cleavage and allied rock structures, with special reference to the mechanical theories of their origin. *Rep. Br. Ass. Advmt. Sci.* 1885 (55th meeting) 813–852.

Hobbs, B. E., Means, W. D. & Williams, P. F. 1976. *An Outline of Structural Geology*. Wiley, New York.

Ildefonse, B., Launeau, P., Bouchez, J. L. & Fernandez, A. 1992. Effect of mechanical interactions on the development of shape preferred orientations: a two-dimensional experimental approach. *J. Struct. Geol.* **14**(1), 73–83.

Lister, G. S. & Williams, P. F. 1983. The partitioning of deformation in flowing rock masses. *Tectonophysics* **92**, 1–33.

Passchier, C. W. 1987. Stable positions of rigid objects in non-coaxial flow—a study in vorticity analysis. *J. Struct. Geol.* **9**, 679–690.

Passchier, C. W. 1988. Analysis of deformation paths in shear zones. *Geol. Rdsch.* **77**, 309–318.

Powell, C. McA & Vernon, R. H. 1978. Growth and rotation history of garnet porphyroblasts with inclusion spirals in a Karakoram schist. *Tectonophysics* **54**, 25–43.

Ramberg, H. 1963. Fluid dynamics of viscous buckling applicable to folding of layered rocks. *Bull. Am. Ass. Petrol. Geol.* **47**, 484–505.

Ramberg, H. 1977. Some remarks on the mechanism of nappe movement. *Geol. För. Stockh. Förh.* 110–117.

Ramberg, H. & Ghosh, S. K. 1977. Rotation and strain of linear and planar structures in three-dimensional progressive deformation. *Tectonophysics* **40**, 309–337.

Ramsay, J. G. 1962. The geometry and mechanics of formation of 'similar' type folds. *J. Geol.* **70**, 309–327.

Ramsay, J. G. 1963. Structure and metamorphism of the Moine and Lewisian rocks of the north-west Caledonides. In: *The British Caledonides*, Oliver & Boyd, U.K. 143–175.

Rosenfeld, J. L. 1970. Rotated garnets in metamorphic rocks. *Geol. Soc. Am Spec. Pap.* **129**.

Schoneveld, C. 1977. A study of some typical inclusion patterns in strongly paracrystalline-rotated garnets. *Tectonophysics* **39**, 453–471.

Skjernaa, L. 1980. Rotation and deformation of randomly oriented planar and linear structures in progressive simple shear. *J. Struct. Geol.* **2**, 101–109.

Spry, A. 1963. The origin and significance of snowball structure in garnet. *J. Petrol.* **4**, 211–222.

Visser, P. and Mancktelow, N. 1992. The rotation of garnet porphyroblasts around a single fold, Lukmanier Pass, Central Alps. *J. Struct. Geol.* **14**, 1193–1202.

Williams, P. F. & Schoneveld, C. 1981. Garnet rotation and the development of axial plane crenulation cleavage. *Tectonophysics* **78**, 307–334.